Real-Time Adaptive Control Allocation applied to a High Performance Aircraft

John B. Davidson*, Frederick J. Lallman†, and W. Thomas Bundick†
NASA Langley Research Center
Hampton, VA 23681

Abstract

This paper presents the development and application of one approach to the control of aircraft with large numbers of control effectors. This approach, referred to as real-time adaptive control allocation, combines a nonlinear method for control allocation with actuator failure detection and isolation. The control allocator maps moment (or angular acceleration) commands into physical control effector commands as functions of individual control effectiveness and availability. The actuator failure detection and isolation algorithm is a model-based approach that uses models of the actuators to predict actuator behavior and an adaptive decision threshold to achieve acceptable false alarm/missed detection rates. This integrated approach provides control reconfiguration when an aircraft is subjected to actuator failure, thereby improving maneuverability and survivability of the degraded aircraft. This method is demonstrated on a next generation military aircraft (Lockheed-Martin Innovative Control Effector) simulation that has been modified to include a novel nonlinear fluid flow control control effector based on passive porosity. Desktop and real-time piloted simulation results demonstrate the performance of this integrated adaptive control allocation approach.

Introduction

Future aircraft are being proposed with many more control effectors than the traditional elevator, aileron, and rudder. Innovative control effectors under study range from thrust vectoring to all-moving wing tips and actuated forebody surfaces to more exotic effectors such as shape-change materials and fluid-flow devices (figure 1). For example, hundreds or even thousands of micro fluid-flow devices could be distributed in arrays across the upper and lower surface of a wing to allow direct control of the wing's boundary layer. Optimal use of this large number of effectors will be challenging, but the potential control power and redundancy offers the flight controls designer freedom to maximize mission performance and enhance survivability.

In particular, reconfigurable control approaches seek to take advantage of this control redundancy to mitigate the deleterious effects of control effector failure or battle damage [Buffington 1998, Brinker 1999, Tallant 1999]. A key element in these approaches is reconfigurable control allocation.

The reconfigurable control allocator [Lallman 1985, Durham 1992, Buffington 1997, Enns 1998] maps moment (or angular acceleration) commands into physical control effector commands as a function of individual control effectiveness and availability. This paper presents the development of an integrated reconfigurable control allocation method which combines a nonlinear method for control allocation with actuator failure detection and isolation (FDI) (figure 2). This integrated approach provides control reconfiguration when an aircraft is subjected to actuator failure, thereby improving maneuverability and survivability of the degraded aircraft. Desktop and real-time piloted simulation are used to demonstrate the performance of this integrated adaptive control allocation approach.

Real-Time Adaptive Control Allocation

The adaptive control allocation is an integrated approach that combines two main elements: a nonlinear control allocation approach and actuator failure detection and isolation. These elements are discussed in more detail in the following sections.

Control Allocation

In general, the forces and moments generated by the control effectors are a function of vehicle flight condition and effector commands. In the case where, at a given flight condition, the control effectiveness is relatively linear with effector command and there is minimal control coupling, the system can be considered as a linear control allocation problem. The linear control allocation problem can be stated as follows. Given the system

$$m_d = B\delta \qquad (1)$$

where m_d = a qx1 desired moment (or angular acceleration) vector, B = the linear control effectiveness matrix, and δ = a mx1 control vector; determine δ to yield a desired m_d. The dimension of δ is assumed to be greater than the dimension of m_d and δ is constrained by $\delta_{\min} \le \delta \le \delta_{\max}$.

* Research Engineer

† Senior Research Engineer

No copyright is asserted in the United States under Title 17, U.S. Code. The U.S. Government has a royalty-free license to exercise all rights under the copyright claimed herein for Governmental purposes.

Weighted Pseudo-Inverse. One solution to the linear allocation problem is given by a weighted pseudo-inverse. The weighted pseudo-inverse is a computationally efficient, closed-form solution that accommodates redundant and/or zero effective controls and allows removing controls from the solution by zeroing the weight associated with that control. The weighted pseudo-inverse solution is obtained by minimizing

$$J = \frac{1}{2}\delta^T W \delta + \lambda^T (m_d - B\delta) \qquad (2)$$

where W is a diagonal positive definite weighting matrix. Taking partial derivatives of J with respect to δ and λ, setting these equal to zero and solving for δ yields

$$\delta = WB^T (BWB^T)^{-1} m_d = B^+ m_d \qquad (3)$$

A common approach is to choose the weighting matrix W to be a diagonal matrix of control position limits squared. This results in a solution that emphasizes highly effective controls while minimizing deflections of controls with reduced effectiveness. Two possible approaches used when controls exceed a constraint are: 1) the individual controls can be clipped at the constraint or 2) the entire control vector can be scaled such that no constraints are violated. The scaling approach results in a solution that preserves the direction (i.e. the balance between pitch, roll, and yaw moments) of the desired moment. In general, a weighted pseudo-inverse solution does not result in a solution that achieves the maximum attainable moment while preserving the direction of the desired moment. This limitation is overcome by employing the weighted pseudo-inverse in a cascaded (multi-pass) approach [Bordignon 1995]. This results in a non-linear solution.

Extended Control Allocation. A limitation of the control-weighted pseudo-inverse method is that it is based on a model of control effectiveness which assumes non-interacting controls with a relatively linear control effectiveness versus control command (deflection) relationship. Future configurations being proposed with large numbers of distributed control effectors have the potential for increases in control power, but may exhibit significant control interactions and nonlinearities. Research is currently being conducted to develop control allocation methods which can be applied to these future configurations. The goal of this effort is to develop methods that include key control interaction effects and can be solved in real-time on flight control computers of the future.

The approach taken here in is to extend the linear model of control effectiveness given by equation (1) to include additional terms to capture first-order control interaction effects and control effectiveness as a function of command magnitude. The extended form is given by

$$m_d = B\delta + B_2 |\delta| + \sum_{\substack{j=1:m \\ i=1:m}} B_{x_{ij}} |\delta_j| \delta_i \qquad (4)$$

where $|\delta|$ = absolute value of the elements of control vector δ and $|\delta_j|$ = absolute value of jth control.

The first term in equation (4) is the linear control effectiveness matrix. The second term models control moment due to deflection magnitude. The third term models the reduction (or increase) in the control effectiveness of the ith control due to the magnitude of deflection of the jth control. Equation (4) can be written in matrix form as

$$m_d = B\delta + B_2 |\delta| + \left(|\delta|^T \otimes I_q \right) B_x \delta \qquad (5)$$

where $\otimes$ denotes the kronecker matrix product and $|\delta|$ = absolute value of the elements of control vector δ.

The solution is obtained by minimizing

$$J = \frac{1}{2}\delta^T W \delta \qquad (6)$$

subject to the constraint given by equation (5), δ is constrained by $\delta_{\min} \le \delta \le \delta_{\max}$ and W is a diagonal positive definite weighting matrix. Numerical optimization methods are being used to determine a control vector δ that minimizes the cost function J. Current solution methods do not reliably run in real-time; therefore, the extended approach was not used in the piloted simulation evaluation.

Actuator Failure Detection and Isolation

Failure Detection and Isolation (FDI) in dynamic systems has been the subject of considerable work for many years [Frank 1990, Patton 1994]. While some approaches employ neural networks, most of the methods developed for FDI involve the use of a model of the system for which failures are being diagnosed, and such is the case with the present approach. In the current application, FDI is used to detect actuator failures.

For this effort it was assumed that the only measurements available from the actuators are the command input and the actuator output, or position. At first thought, it might seem that a failure of the actuator could simply be detected by comparing the measured position with the command, and, if these are different, a

failure has occurred. However, because of the dynamic response of the actuator, the output will differ from the command during most transients, and thus false failures will be declared unless the threshold for failure declaration is set unacceptably high. This problem is overcome in a model-based FDI approach by using a model of the actuator in the FDI system to predict actuator behavior as in figure 3, and by comparing the model output with the measured actuator position. If the model is perfect, the no-failure residual will be zero. Thus, a failure is declared when the residual is not zero. Nominal measurement errors are accommodated by using a non-zero decision threshold for comparison with the residual. However, if model errors are significant, residuals can be quite different from zero. In fact, they can be so large that a constant threshold must be set so high to minimize false alarms that the missed detection rate is unacceptable. In this case, acceptable false alarm/missed detection rates can often be achieved by use of an adaptive decision threshold. If the actuator and its model are linear, the residual caused by model error is a linear function of the input amplitude, and the adaptive threshold can vary linearly with the amplitude of the input. For actuators which are nonlinear due to limiting, generating an adaptive threshold as a function of a composite signal, which at each sample is the maximum of the real-time and delayed versions of the command provides much improved false alarm/missed detection performance. In the current work the adaptive threshold was implemented in the following form

$$th = \begin{cases} a + b\max\left(\left|\delta_{cmd}\right|, \left|\delta_{dly}\right|\right) \\ \quad + cu\left(\max\left(\left|\dot{\delta}_{cmd}\right|, \left|\dot{\delta}_{dly}\right|\right) - d\right) & \left|\delta_{cmd}\right| \le \delta_{\lim} \\ a + b\delta_{\lim} \\ \quad + cu\left(\max\left(\left|\dot{\delta}_{cmd}\right|, \left|\dot{\delta}_{dly}\right|\right) - d\right) & \left|\delta_{cmd}\right| > \delta_{\lim} \end{cases}$$

where u(•)=unit step function.

An example of the adaptive threshold behavior can be seen in figures 4 through 6. These data were generated in the stand-alone desktop simulation of an actuator. Figure 4 shows the actuator position, and the amount of surface activity that is typical of a maneuvering high performance aircraft. Note that the actuator failed at its current position at about 35.8 seconds. Figure 5 is a plot of the adaptive threshold and the absolute value of the residual for this case and shows the increased residual after the failure. Figure 6 is a time-expanded version of figure 5 showing that the no-failure residual near 15 seconds would have produced a false alarm had not the threshold adapted. This increase in residual was caused by a model inaccuracy in the actuator rate limit.

The actuator model used in the FDI system is a discrete second-order model with position and rate limits. The model output is subtracted from the measured actuator position to form the residual. To simulate model errors, values of the actuator parameters were varied to determine their effects on the residuals. It was found that amplitude of the residuals due to model error (no failures) was determined primarily by errors in the position and rate limit models with errors in the natural frequency and damping being secondary. To obtain a quantitative measure of the effect of input amplitude on the amplitude of the no-failure residuals, a Monte Carlo analysis was conducted using a stand-alone MATLAB/Simulink[+]-based simulation of the actuator and the FDI system (figure 7). Actuator position and rate limits and measurement errors were randomly varied run-to-run as were the amplitudes of the command inputs. The range of variation of the rate limit was chosen based on the rate limit versus hinge-moment model of the actuators in a current fighter aircraft. Analysis of these results were used to determine the parameter values of the current adaptive-threshold actuator FDI design.

Implementation

The integrated Control Allocator is organized into five main elements (see Figure 8): Command Interconnect, Effector Aero Model, Control Mixer, Control Distributor, and the Actuator FDI. These elements are discussed in the following.

The Command Interconnect maps stability-axis rotational acceleration commands into desired body-axis moments and provides inertial coupling compensation. The Effector Aero Model contains linearized control effectiveness coefficients as a function of flight condition. The control mixer contains the control allocation algorithm. Two algorithms are currently under study – a position limit weighted pseudo-inverse and the extended control allocation. The Control Distributor maps control commands to the individual control effectors.

Left and right one-sided controls are modeled as a single control in the Aero Model and the Mixer and are mapped into left and right surface commands in the Control Distributor. During nominal operation, the allocator distributes the controls based upon the internal model of the individual control effectiveness as a function of flight condition.

The control allocator accepts inputs from the Actuator Failure Detection element, which continually monitors the health of the control surface actuators. When informed by the FDI that an actuator failure has

[+] The Mathworks, Inc.

occurred, the allocator removes the failed control from the set of available controls and redistributes the remaining controls to accommodate the failure.

Application to ICE Aircraft

This integrated allocation method has been implemented in a modified version of the Lockheed-Martin Innovative Control Effector (LM-ICE) simulation [Dorsett 1996]. The LM-ICE aircraft is a 65 degree swept delta-wing, tailless, single-engine, supersonic fighter. This configuration incorporates a large number of redundant conventional and innovative control effectors including elevons, pitch flaps, pitch and yaw thrust vectoring, all-moving wing tips (AMT's), spoiler-slot deflectors (SSD's), and outboard leading-edge flaps (OLEF's) (figure 9).

This simulation has been modified to include a new control effector based on passive porosity [Hunter 2001]. Passive Porosity (PassPort), as used in this study, is a control device that changes aerodynamic forces on a vehicle wing by equalizing the pressure gradient on the exterior surface. Actuation is accomplished by opening and closing a minimum depth cavity (plenum) (figure 10a). The plenum is designed with a porous surface conforming to the wing shape. For this study, eight separate devices were installed on each wing (figure 10b). The controller actuates each device discretely to an "on" or "off " position. No control interaction data is currently available for the passive porosity, therefore it was assumed that the use of the passive porosity had no effect on the moments produced by the other controls.

An example of one of the control interaction effects exhibited by the ICE aircraft is shown in figure 11. Due to its location, deflection of the spoiler-slot deflector can significantly effect the forces and moments produced by the elevons and pitch flap, as illustrated in the figure. This figure shows aerodynamic pitch (11a) and roll (11b) moment coefficients for the right elevon and spoiler-slot deflector as a function of angle-of-attack at a low speed flight condition. The plots show elevon effectiveness for +/-30 degree elevon deflection with the spoiler-slot deflector at 0 and 45 degrees. The spoiler-slot deflector pitch and roll effectiveness is also plotted for comparison with the elevon. At low angles-of-attack, the elevon pitch and roll moments are significantly reduced (by approximately 60%) by deflection of the spoiler-slot deflector.

All actuators are simulated as second-order systems with rate and position limits except the passive porosity actuator. Dynamic data is currently not available for passive porosity. The actuator was chosen to be modeled by a position and rate-limited first-order system. Actuator dynamics and limits are given in Table 1.

The control law is designed to give conventional responses to three-axis pilot controls. Pitch rate, roll rate and sideslip angle commands are scheduled with the available control power in each axis.

The longitudinal control law is a proportional-plus-integral arrangement with feed-forward that produces a pitch acceleration command for the control allocator. Longitudinal control stick deflections command pitch rate at low speed. The control law transitions to normal acceleration command at high speed. Feedback gains were chosen following the guidance of MIL-STD-1797A for short-period frequency and damping ratio. Attitude angles are used to compensate for gravity. Roll rate and the angle of sideslip are used to compensate for pitch rate sensor offsets that occur when the airplane rolls with sideslip.

Lateral control stick deflections command stability-axis roll rate by means of a single feedback gain on roll rate error. Rudder pedal deflections command the angle of sideslip by means of a proportional-plus-derivative controller. Sideslip error feedback provides static directional stability. Stability-axis yaw rate combined with attitude angles and lateral acceleration to form a synthesized rate-of-change of sideslip that provides yaw damping. Phase margins in both the longitudinal and lateral-directional channels are enhanced by lead filters.

Initial control system gains were obtained using frequency-domain design techniques on a set of continuous models. The models range from Mach 0.225 to Mach 0.9 with altitudes ranging from sea level to 40,000 feet. The control law was discretized and tested for large-amplitude motions on a nonlinear desktop simulation. Additional refinements were made in response to piloted simulation results.

The Effector Aero Model for the allocator contains pitch, roll, and yaw moment effectiveness coefficients for each control as a function of flight condition. The coefficients were calculated for controls at full positive and negative deflections using piece-wise linear fits of the ice database.

An example is presented to demonstrate the performance of the extended allocation approach at a flight condition with significant control interactions. The control effectiveness of the ICE aircraft at a low speed flight condition can be modeled using the extended approach by

$$m = B\delta + B_2 |\delta| + B_{x_{ssd}} |\delta_{ssd}| \delta \quad (7)$$

where

$$\delta = \begin{bmatrix} \delta_{le} & \delta_{re} & \delta_{amt} & \delta_{ptv} & \delta_{ytv} & \delta_{pp} & \delta_{pf} & \delta_{ssd} \end{bmatrix}^T$$

and *le* = left elevon, *re* = right elevon, *amt* = all-moving wing tip, *ptv* = pitch thrust vectoring, *ytv* = yaw thrust

vectoring, *pp* = passive porosity, *pf* = pitch flap, and *ssd* = spoiler-slot deflector.

The first term in equation (7) is the linear control effectiveness matrix. The second term models pitch moment due to deflection of the all-moving wing tip and spoiler-slot deflector. The third term models the reduction in the control effectiveness of the left elevon, right elevon, and pitch flap due to deflection of the spoiler-slot deflector. The control effectiveness and coupling matrices are given in Table 2.

For comparison, the desired control-moment vector m_d was allocated among the control effectors using a cascaded pseudo-inverse approach and using the extended linear approach, where the desired moment vector (pitch moment, roll moment, yaw moment) is

$$m_d = \begin{bmatrix} 0 & 50000 & 100000 \end{bmatrix}^T$$

The weighting matrix *W* was set to identity. The extended linear solution was determined using the MATLAB constrained optimization routine (CONSTR). The control deflections resulting from the two approaches are shown in figure 12. The control moments achieved by applying these control deflection solutions to the nonlinear aero model are given in figure 13. As can be seen, by including control interaction effects the extended linear solution results in a better match to the desired moment.

Desktop and Piloted Simulation Evaluation

Desktop and piloted simulations are currently being conducted to evaluate and refine the approach. The desktop simulation is implemented in MATLAB/Simulink+. Piloted simulations are being conducted in NASA Langley's Differential Maneuvering Simulator (DMS). The DMS is a fixed-base generic fighter simulator having wide-angle visual displays and is capable of simulating two airplanes as they maneuver relative to each other.

For the piloted simulation evaluations, a control weighted pseudo inverse allocation approach was used with the actuator FDI. The SSD and OLEF's were not used.

The response of the actuator FDI system to an elevon failure at 10 seconds in one of the piloted simulation runs is plotted in figure 14. The FDI system detected the failure in 0.0625 seconds, and the control allocator removed the surface from use on the next computational cycle. This was typical of the FDI performance in the piloted simulations.

Pilot-in-the-loop tracking tasks were conducted to assess the performance of the integrated control allocation approach. Test subjects performed a gunsight tracking task using a pre-recorded maneuvering target projected on the simulator dome. The attack aircraft starts at an initial condition of Mach=0.6, altitude=11700 feet, in straight and level flight. The target aircraft starts at the same initial condition and 500 feet ahead of the attack aircraft. The target performs a series of roll reversals with conditions varying between 300-500 knots-equivalent-airspeed, 9500-12200 feet in altitude, and 1-7 g's. Pilot tracking performance was measured by target cone angle ε, defined as the angle between the attacking aircraft's x-body axis and a vector from the attacker to the target. (figure 15) [Foster 1998]. Pilot tracking time histories are given in figure 16 for a left elevon failure at 15 sec with FDI On (16a) and FDI Off (16b). Both sets of time histories are plotted against a baseline tracking case with no failures. As can be seen in figure 16a, the FDI On with failure time histories compare very favorably to the baseline both in terms of stick activity and target cone angle. In this case the allocator, advised of the failure by the FDI, compensates by redistributing the commands to the remaining functioning effectors. Pilot comments for this case were: "slightly more oscillatory (than baseline)", "minor increase in workload", "good tracking". Figure 16b shows FDI Off with failure time histories compared to the baseline. In this case the allocator is ignorant of the failure. Time histories show more stick activity and significantly larger target cone angle. Pilot comments for this case were: "major increase in workload (after failure)", "unable to track target". The simulation results demonstrate that the integrated control allocator is able to reconfigure after actuator failures to allow the tracking task to be completed.

Concluding Remarks

This paper has presented the development of a real-time adaptive control allocation approach. The integrated approach combines a nonlinear approach to control allocation, with actuator failure detection and isolation. This integrated approach provides control reconfiguration when subjected to actuator failure, thereby improving the degraded aircraft's maneuverability and survivability. This paper also addressed system implementation issues. The method has been demonstrated on a Lockheed-Martin Innovative Control Effector simulation that has been modified to include actuated passive porosity. Desktop and real-time piloted simulation results demonstrate the performance of this integrated reconfigurable control allocation approach.

In the next phase of this work a real-time parameter identification module, currently in development, will be integrated into the system. Also in development are a parity-space-based FDI module for detecting and

+ The Mathworks, Inc.

isolating failures in redundant flight control sensors, a cascaded pseudo-inverse implementation of frequency-apportioned control allocation, and incorporation of additional unconventional control effectors, such as fluidic thrust vectoring and synthetic jets. Additional research is also required to develop improved modeling of control effector interactions and reliable and efficient solution methods to enable non-linear real-time control allocation.

References

Aeronautical Systems Division, Air Force Systems Command, "Military Specification - Flying Qualities of Piloted Vehicles," MIL-STD-1797A, January 1990.

Bordignon, K. and Durham, W.: Closed-Form Solutions to Constrained Control Allocation Problem. *J. of Guidance Control and Dynamics*. Vol.18, No.5, 1995.

Brinker, J.S. and Wise, K.A.: Reconfigurable Systems for a Tailless Fighter Aircraft - Restore. AFRL-VA-WP-TR-1999-3067, 1999.

Buffington, J.: Tailless Aircraft Control Allocation. AIAA-97-3605.

Buffington, J.; Chandler, P.; and Pachter, M.: Integration of On-line System Identification and Optimization-based Control Allocation. AIAA-98-4487.

Dorsett, K. and Mehl, D.: Innovative Control Effectors (ICE). WL-TR-96-3043, January 1996.

Durham, W.: Constrained Control Allocation. AIAA-92-4550.

Enns, D.: Control Allocation Approaches. AIAA-98-4109.

Frank, P.M.: Fault Diagnosis in Dynamic Systems Using Analytical and Knowledge-based Redundance - A Survey and Some New Results. *Automatica*, vol. 26, no. 3, 1990, pp. 459-474.

Foster J.V.; Ross, H.M.; Brown, P.W.; Rivers, R.A.; et al.: Piloted Simulation Study of High-Angle-of-Attack Roll-Maneuvering Criteria for Fighter Airplanes. NASA TP-1998-208727.

Graham, A., *Kronecker Products and Matrix Calculus: with Application*, John Wiley and Sons, New York, 1981.

Hunter, C.A.; Viken, S.A.; Wood, R.M.; and Bauer, S.X.S.: Advanced Aerodynamic Design of Passive Porosity Control effectors. AIAA 2001-0249.

Lallman, F.J.: Relative Control Effectiveness Technique with Application to Airplane Control Coordination. NASA TP-2416, 1985.

Patton, R. J.: Robust Model-based Fault Diagnosis: The State of the Art. *IFAC/INACS Symp. on Fault Detection, Supervision, and Safety for Technical Processes -SAFEPROCESS '94*, 1994.

Tallant, G.S.; Niestroy, M.A.; Eberhardt, R.L.; Monaco, J.F.; and Ward, D.G.: Reconfigurable Systems for Tailless Fighter Aircraft – Restore. AFRL-VA-WP-TR-1999-3078, 1999.

Wood R. M. and Bauer S.X.: Advanced Aerodynamic Control Effectors. SAE 1999-01-5619, 1999.

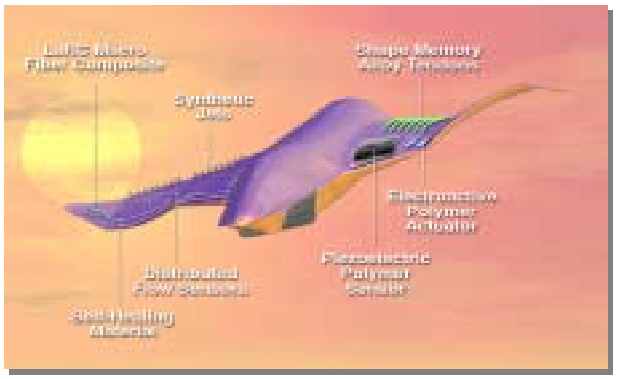

Figure 1. Future Aircraft with Distributed Array of Micro Fluid-Flow Control Effectors.

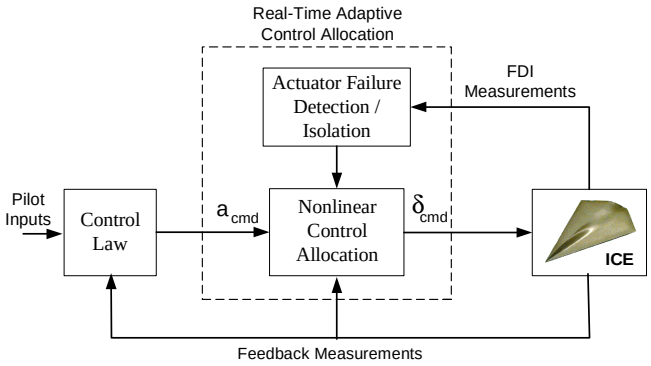

Figure 2. Real-Time Adaptive Control Allocation.

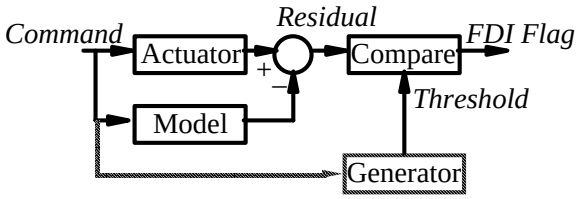

Figure 3. Actuator Failure Detection and Isolation.

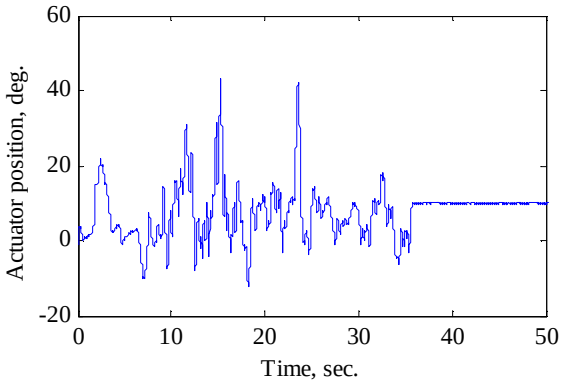

Figure 4. Failed Actuator Position.

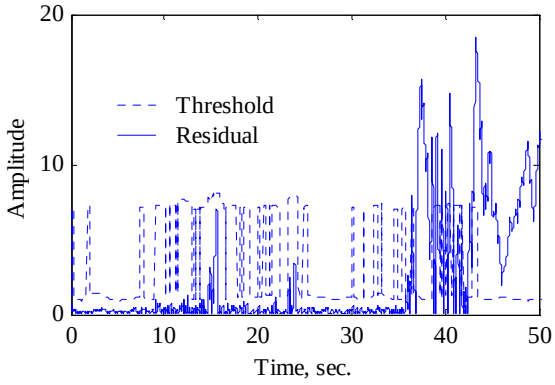

Figure 5. FDI Threshold and Residual for Failed Actuator.

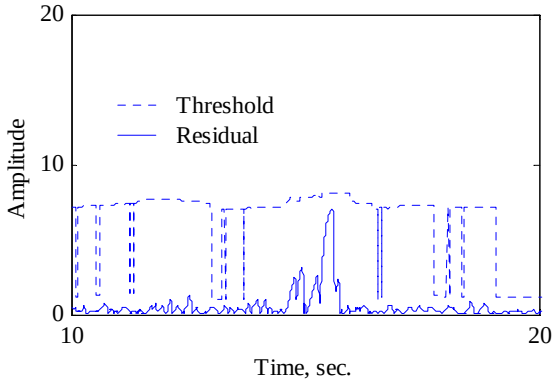

Figure 6. Expanded View of Threshold and Residual.

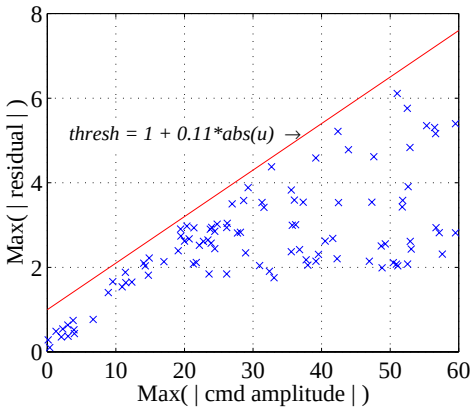

Figure 7. Monte Carlo Analysis for Adaptive-Threshold FDI Design.

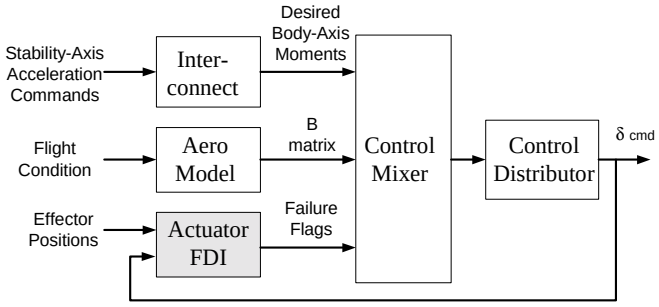

Figure 8. Integrated Adaptive Control Allocation Implementation.

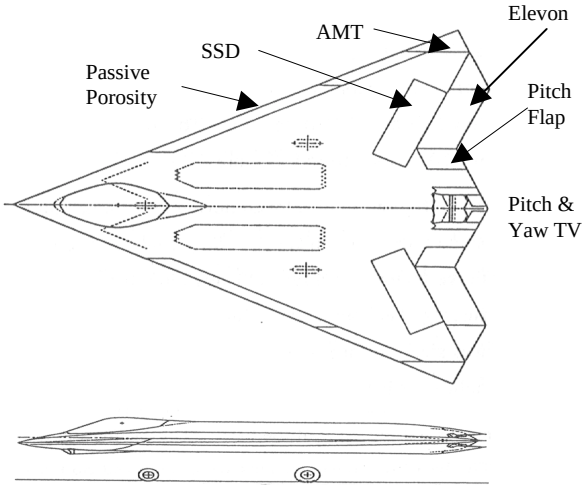

- Advanced tailless, delta wing configuration
  Low radar signature, high agility
  Aero data for $0.3<M<2.16$, $-4.0<\alpha<90.0$, $-30.0<\beta<30.0$
- Simulation includes increments for steady rotations, controls, control interactions, hinge moments
- Innovative Control Effectors (ICE)
  Pitch and yaw Thrust-Vectoring (TV), elevons, pitch flaps, all-moving wing tips (AMT's), spoiler-slot deflectors (SSD's), differential leading edge flaps (DLEF's) [Dorsett 1996]
- Nominal configuration modified to include actively controlled passive porosity effectors

Figure 9. Modified Lockheed-Martin Innovative Control Effector (ICE) Configuration. (Aircraft Figure from Dorsett 1996.)

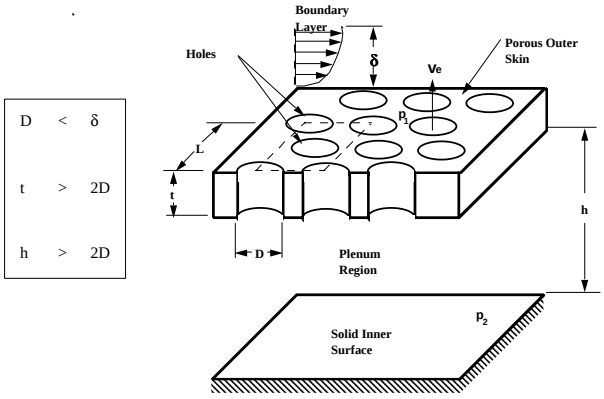

Figure 10a. Schematic of Passive Porosity Effector. (Figure from Wood 1999.)

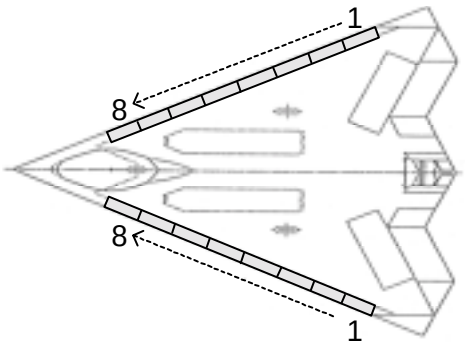

Figure 10b. Passive Porosity on ICE.

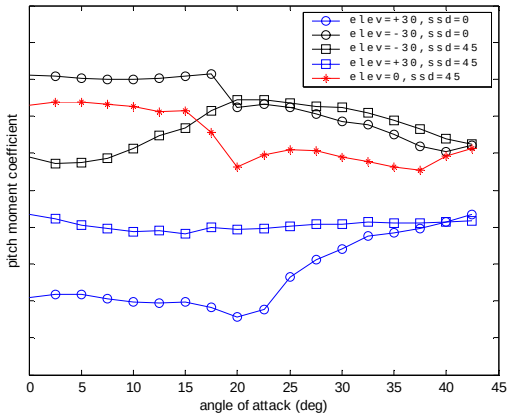

Figure 11a. Pitch Moment Coefficient – Elevon and Spoiler-Slot Deflector.

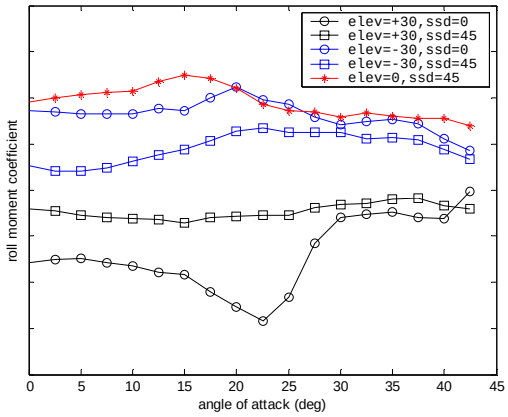

Figure 11b. Roll Moment Coefficient – Elevon and Spoiler-Slot Deflector.

Table 1. Effector Dynamics and Limits.

Effector	Dynamics (freq (r/s), damping)	Position Limit (deg)	Rate Limit (deg/sec)
Elevon	(63.246 , 1.107)	-30 / +30	150
AMT	(63.246 , 1.107)	0 / 60	150
Pitch TV	(39.189 , 1.001)	-15 / +15	60
Yaw TV	(39.142 , 1.001)	-15 / +15	60
Passive Pososity*	80.0	0 / 8	40
Pitch Flap	(63.246 , 1.107)	-30 / +30	50

* First order model

Table 2. Control Effectiveness and Coupling Matrices.

$$B = \begin{bmatrix} -3368.4 & -3368.4 & 0 & -1089.8 & 0 & 0 & -2698.6 & 0 \\ 2268.1 & -2268.1 & 1531.9 & 0 & 0 & 6395.1 & 0 & 1929.7 \\ 95.7 & -95.7 & -443.6 & 0 & -1089.8 & 1162.7 & 0 & 1516.8 \end{bmatrix}$$

$$B_2 = \begin{bmatrix} 0 & 0 & 1020.0 & 0 & 0 & 0 & 0 & 1548.3 \\ 0 & 0 & 0 & 0 & 0 & 0 & 0 & 0 \\ 0 & 0 & 0 & 0 & 0 & 0 & 0 & 0 \end{bmatrix}$$

$$B_{x_{ssd}} = \begin{bmatrix} 74.09 & 74.09 & 0 & 0 & 0 & 0 & -2.8 & 0 \\ 49.8 & 49.8 & 0 & 0 & 0 & 0 & 0 & 0 \\ 0 & 0 & 0 & 0 & 0 & 0 & -0.9 & 0 \end{bmatrix}$$

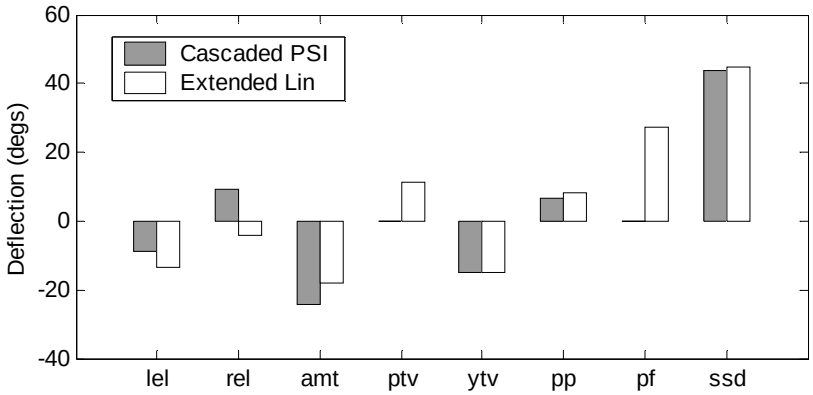

Figure 12. Control Deflections – Cascaded Pseudo-Inverse and Extended Linear Approaches.

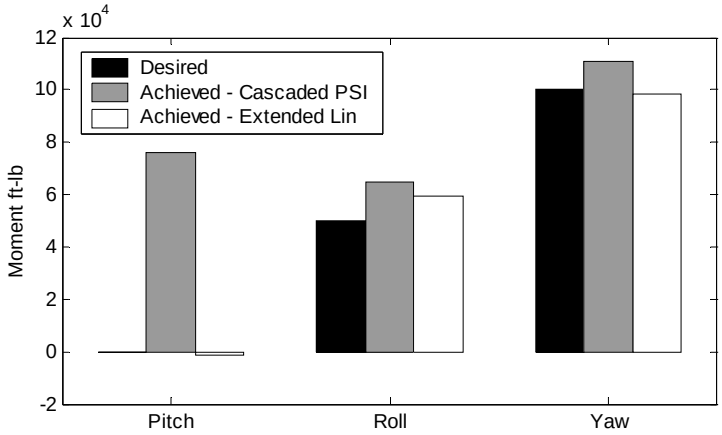

Figure 13. Desired and Achieved Control Moments
– Cascaded Pseudo-Inverse and Extended Linear Approaches.

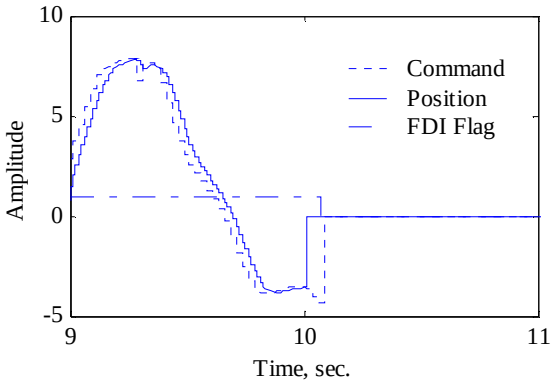

Figure 14. Elevon Failure Detection in Piloted Simulation.

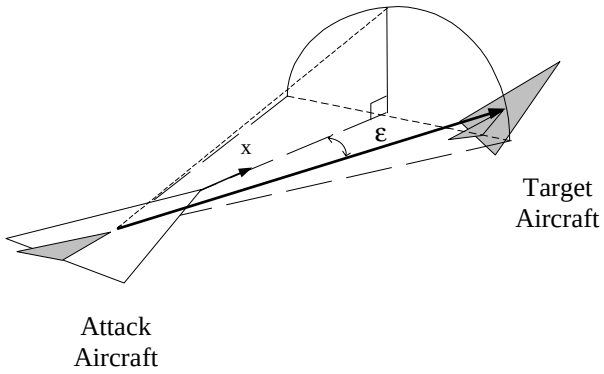

Figure 15. Target cone angle, ε.
(Figure from Foster 1998.)

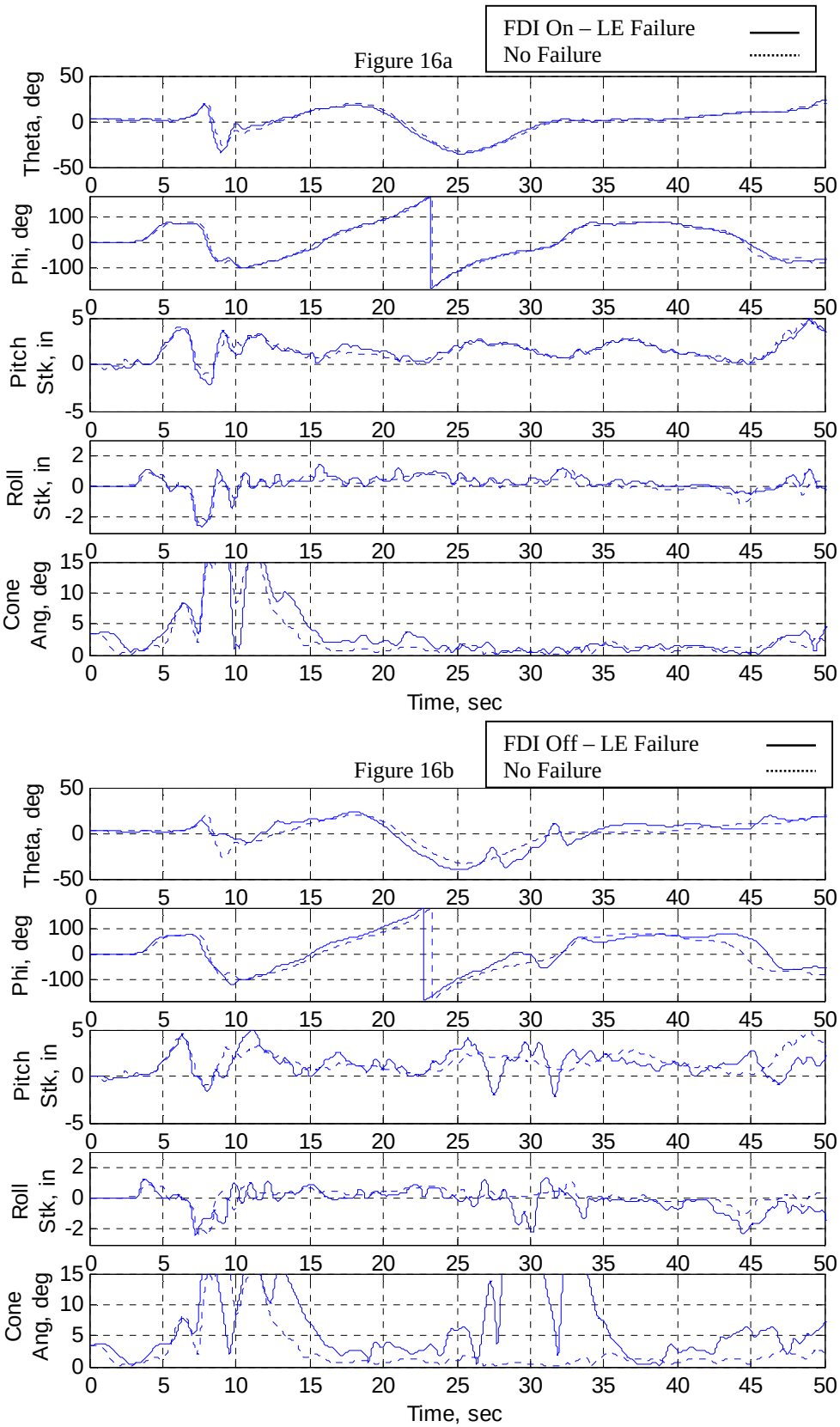

Figure 16. Piloted Target Tracking Time Responses – Left Elevon Failure at 15 sec, FDI On (16a) and FDI Off (16b).